Formation of Electron-Root Radial Electric Field and its Effect on Thermal Transport in LHD High T_e Plasma

Seikichi MATSUOKA[a], Shinsuke SATAKE, Hiromi TAKAHASHI, Arimitsu WAKASA[1], Masayuki YOKOYAMA, Takeshi IDO, Akihiro SHIMIZU, Takashi SHIMOZUMA, Sadayoshi MURAKAMI[1] and LHD Experiment Group

National Institute for Fusion Science, Toki 509-5292, Japan

[1]*Department of Nuclear Engineering, Kyoto University, Kyoto 606-8501, Japan*

(Received 17 July 2012 / Accepted 5 March 2013)

Neoclassical transport analyses have been performed for a high electron temperature LHD plasma with steep temperature gradient using a neoclassical transport simulation code, FORTEC-3D. It is shown that the large positive radial electric field is spontaneously formed at the core along with the increase in the electron temperature, while the neoclassical heat diffusivity remains almost unchanged. This indicates that the $1/\nu$-type increase expected in the neoclassical transport in helical plasmas can be avoided by the spontaneous formation of the radial electric field. At the same time, it is found that the experimentally estimated heat diffusivity is significantly reduced. This suggests that the formation process of the transport barrier in the high electron temperature plasma can be caused by the spontaneous formation of the radial electric field.

Keywords: radial electric field, finite orbit width effect, neoclassical transport, δf Monte Carlo simulation

DOI: 10.1585/pfr.8.1403039

1. Introduction

The formation of the electron internal transport barrier (eITB) observed in many helical devices [1, 2] is promising for the better confinement. High electron temperature (T_e) plasmas followed by the formation of the eITB are called CERC (Core Electron-Root Confinement) plasmas since they have a large positive (electron-root) radial electric field (E_r) at the plasma core. It has been observed that the E_r in a CERC plasma has a steep shear at the plasma core region where the steep T_e gradient of eITB forms. In the Large Helical Device (LHD), CERC plasmas are originally observed in the NBI-sustained plasmas with a superposition of electron cyclotron heating (ECH) [3]. Recent experiments in LHD have shown that the high T_e plasmas can be observed with only ECH for relatively low density plasmas [4].

During the discharge of a CERC plasma, it has been observed in LHD that the T_e profile changes from flat into steep one as the ECH continues. In this process, a locally flat profile of T_e appears temporally, then the local flat region shrinks, and finally the T_e profile results in the steep eITB one. The resultant foot point of the eITB approaches the low order rational surface of $\iota/2\pi = 1/2$. It has been pointed out that the position where the eITB formation occurs in CERC plasmas has a close relationship to either a low-order rational surface or a magnetic island [5]. It has been also reported that there is a threshold of the heating power to realize the electron-root E_r, and it has a clear dependence on the magnetic axis position [6]. With these observations, however, the mechanism of the eITB formation has not been clarified. It is necessary to understand the mechanism how the eITB forms from the viewpoint of the transport. In general, the E_r and its shear strongly affect both the neoclassical and anomalous transport. Since CERC plasmas are characterized by the formation of the electron-root E_r at the core, it is important at first to investigate the E_r formation process and its relation to the transport reduction during the discharge. The E_r in helical plasmas can be determined by the ambipolar condition of the neoclassical transport, where the neoclassical particle fluxes of the electron and the ion balance. An accurate evaluation of the neoclassical transport and E_r is a key issue in the transport studies in helical plasmas.

In our recent work, it has been shown that the finite drift motion of electron orbits across the field lines, or the finite orbit width (FOW) effect on the neoclassical transport becomes important in high T_e helical plasmas due to the large deviation of the helically-trapped electrons [7]. A neoclassical transport code, FORTEC-3D, which was used in that study, has been developed with the aim to apply to such high T_e plasmas. FORTEC-3D code has features below: (1) it involves the electron FOW effect in following the orbit of (marker) particles with the δf Monte Carlo approach, (2) it can be applied to arbitrary magnetic field configurations such as tokamaks and helical/stellarator plasmas when the field is expressed in Boozer coordinates [8],

author's e-mail: matsuoka@rist.or.jp

[a] Present address: Research Organization for Information Science and Technology, Kobe 650-0046, Japan.

(3) the collision operator for like-particles satisfies the elementary conservation laws for the particle number, the momentum, and the total energy, and (4) the steady-state ambipolar E_r is determined self-consistently by the ambipolar condition of Eq. (4) shown later. It is noted that the collision operator for unlike-species (here, the electron-ion collision) is represented only by the Lorentz operator, or the pitch angle scattering, since ion is assumed to be a stationary Maxwellian. This is due to the fact that any external momentum input for the ion does not exist, and thus the ion mean flow can be regarded negligible compared to the electron thermal speed. Although the momentum conservation in the unlike-particle collision is not satisfied for the collision operator, momentum transfer from electron to ion is negligible due to the large difference between the electron mass and ion one. With these features, FORTEC-3D code is aimed to evaluate the neoclassical transport and the ambipolar E_r more accurately in high temperature plasmas.

In this paper, FORTEC-3D code is applied to a LHD CERC plasma to clarify characteristics in the formation of E_r and its effect on the electron thermal transport. we show that the ambipolar E_r spontaneously grows to have a large positive electron root with the steep shear as the T_e gets high and the eITB formation proceeds. On the other hand, the electron neoclassical heat diffusivities remain almost constant due to the electron-root E_r. It is kept lower level than expected from the so-called $1/\nu$ scaling in which the heat diffusivity increases in proportion to $T_\mathrm{e}^{7/2}$ in helical plasmas. It indicates that the spontaneous formation of the electron-root E_r compensates the increase in the electron thermal transport in the CERC plasma. The experimental heat diffusivities estimated from the input power of the ECH is compared to the neoclassical ones.

The rest of this paper is organized as follows. In Sec. 2, the brief description of a numerical neoclassical transport code, FORTEC-3D, and the ambipolar condition for the E_r is presented. The importance of the electron FOW effect on the electron neoclassical transport is also described in this section. Section 3 gives numerical results of neoclassical transport analyses for a LHD CERC plasma. Finally, a summary and a discussion are given in Sec. 4.

2. Neoclassical Transport Code with Finite Orbit Width Effect, FORTEC-3D

FORTEC-3D solves the drift kinetic equation based on the two-weight δf Monte Carlo method [9–11]. It determines the neoclassical particle and energy fluxes by following the motion of a large number of marker particles in an arbitrary magnetic field. In the two-weight δf Monte Carlo method, the distribution function f_a is decomposed into two parts as $f_a = f_{a,0} + \delta f_a$, where a = e, i denotes a plasma species and $f_{a,0} = f_{a,\mathrm{M}}$ is the Maxwellian distribution function. The following drift kinetic equation for the δf_a part of the distribution should be solved using simulation markers,

$$\begin{aligned} \frac{D\delta f_a}{Dt} &\equiv \left[\frac{\partial}{\partial t} + (\boldsymbol{v}_\parallel + \boldsymbol{v}_\mathrm{d})\cdot\nabla + \dot{K}\frac{\partial}{\partial K} - C_\mathrm{TP}\right]\delta f_a \\ &= \left[-(\boldsymbol{v}_\parallel + \boldsymbol{v}_\mathrm{d})\cdot\nabla + C_\mathrm{FP}\right] f_{a,\mathrm{M}}, \end{aligned} \tag{1}$$

where $\boldsymbol{v}_\parallel$ and $\boldsymbol{v}_\mathrm{d}$ are the parallel and drift velocity of particles, and C_TP and C_FP are the test particle and field particle collision operators, respectively. In FORTEC-3D, the electron-electron collision operator satisfies the conservation laws for the particle number, momentum, and the total energy (see Ref. [11]), while the electron-ion one only involves the pitch angle scattering. The assumption that the ion distribution function is a stationary Maxwellian and its mean flow U_i is negligibly small compared with the electron thermal speed, $v_\mathrm{th,e} \gg v_\mathrm{th,i} \simeq U_\mathrm{i} \simeq 0$, enables FORTEC-3D to use such simplified collision operator for the electron-ion collision, where $v_\mathrm{th,e}$ and $v_\mathrm{th,i}$ are the electron and ion thermal velocities, respectively. The five-dimensional phase space variables, $(\boldsymbol{R}, K, \mu)$, are used here, where $\boldsymbol{R}$ represents the position vector in Boozer coordinates, K is the kinetic energy, and μ is the magnetic moment. The $f_{a,0} = f_{a,\mathrm{M}}$ does not have the mean velocity here, and thus it does not contribute to any radial transport. Hence, the neoclassical transport in the radial direction is only obtained by moments of the δf in velocity spaces. The neoclassical radial particle and energy fluxes $\mathit{\Gamma}_a$ and Q_a are given as follows:

$$\mathit{\Gamma}_a = \int v_\mathrm{r}\, \delta f_a\, \mathrm{d}^3 v, \tag{2}$$

$$Q_a = \int \frac{1}{2} m_a v^2 v_\mathrm{r}\, \delta f_a\, \mathrm{d}^3 v, \tag{3}$$

where v and v_r are the velocity and its radial component, and m_a is the mass of a-th species.

In referring to the FOW effect in this paper, we mean the whole effect caused by neglecting the particle radial drift. This comes from the convention of the *local* neoclassical transport adopted in many numerical neoclassical transport codes, such as DKES [12]. In the *local* codes, not only the radial drift but also the ∇B and curvature drifts in poloidal and toroidal directions included in the drift kinetic equation are neglected as a consequence of the assumption of $|v_{\boldsymbol{E}\times\boldsymbol{B}}| \gg |v_{\boldsymbol{B}}|$, where $v_{\boldsymbol{E}\times\boldsymbol{B}}$ is the $\boldsymbol{E}\times\boldsymbol{B}$ drifts and $v_{\boldsymbol{B}}$ represents the drift arising from the ∇B and the curvature. It is noted that the incompressible $v_{\boldsymbol{E}\times\boldsymbol{B}}$ is also usually assumed there. These assumptions are not necessary for FORTEC-3D since all the drifts above are included in FORTEC-3D. The FOW effect on the neoclassical transport arises through the collisionless detrapping of the helically-trapped particles and the poloidal resonance. The former one makes the $1/\nu$ neoclassical transport flux smaller due to the less fraction of the helically-trapped particles as a consequence of the collisionless detrapping of trapped particles. With the latter effect, the neoclassical transport flux of purely $1/\nu$-behavior appears with a small but finite E_r. More detailed discussion on the electron FOW effect can be seen in Ref. [7].

In this paper, only the electron neoclassical transport is evaluated by FORTEC-3D with its FOW taken into account. The reason for this is twofold: one is that the electron FOW effect makes a significant influence on the electron neoclassical transport when T_e is high due to helically-trapped particles in a three-dimensional magnetic field [7] and the other is that the ion temperature is in general low in CERC plasmas.

The time evolution of E_r can be described by the following equation,

$$\epsilon_\perp \epsilon_0 \frac{\partial E_\mathrm{r}}{\partial t} = -e\left\{\mathit{\Gamma}_\mathrm{e}(E_\mathrm{r}, U_{\mathrm{e},\parallel}) - \mathit{\Gamma}_\mathrm{i}(E_\mathrm{r}, U_{\mathrm{i},\parallel})\right\}, \qquad (4)$$

where $U_{a,\parallel}$ is the parallel mean flow of species a, ϵ_0 represents the electric permittivity in the vacuum, and $\epsilon_\perp$ denotes the effect of the classical polarization current defined by

$$\epsilon_\perp \equiv \langle|\nabla\rho|^2\rangle + \left\langle \frac{v_\mathrm{A}^2}{c^2}|\nabla\rho|^2 \right\rangle, \qquad (5)$$

where v_A is the Alfvèn velocity and c is the speed of light. The radial electric field is determined in FORTEC-3D by imposing the ambipolar condition for the neoclassical particle fluxes of electrons and ions. It is realized when the left hand side of Eq. (4) vanishes: $\mathit{\Gamma}_\mathrm{e}$ and $\mathit{\Gamma}_\mathrm{i}$ balance and E_r reaches a steady state. Hence, one needs to evaluate the ion neoclassical particle flux in addition to the electron one although only the latter is evaluated by FORTEC-3D in this paper. Since it requires the large amount of computational resources to simultaneously calculate both the ion and the electron neoclassical transport fluxes by FORTEC-3D, a database made by DGN/LHD [13], which is a numerical neoclassical transport code without the FOW effect, is adopted for the ion particle flux as is done in the reference [14]. The ion particle flux $\mathit{\Gamma}_\mathrm{i}$ is referred to from the corresponding radial position ρ and the radial electric field E_r. This enables ones to evaluate $\mathit{\Gamma}_\mathrm{i}$ at each time step without much computational burden. Therefore, the E_r is determined by FORTEC-3D to meet the ambipolar condition of $\mathit{\Gamma}_\mathrm{e}^\mathrm{F3D}(E_\mathrm{r}^\mathrm{F3D}) - \mathit{\Gamma}_\mathrm{i}^\mathrm{DGN}(E_\mathrm{r}^\mathrm{F3D}) = 0$, where the superscripts of F3D and DGN refer to the value obtained by FORTEC-3D and DGN/LHD, respectively. It is noted that the E_r can also be determined by using only DGN/LHD as $\mathit{\Gamma}_\mathrm{e}^\mathrm{DGN}(E_\mathrm{r}^\mathrm{DGN}) - \mathit{\Gamma}_\mathrm{i}^\mathrm{DGN}(E_\mathrm{r}^\mathrm{DGN}) = 0$, and the $E_\mathrm{r}^\mathrm{DGN}$ such obtained by DGN/LHD is also shown in the next section for the reference purpose. Finally, it is noted that the averages over certain time steps for resultant values of FORTEC-3D such as E_r, the heat diffusivity, etc., are shown in the remaining part of the paper to remove an inevitable numerical noise of the Monte Carlo method as much as possible.

3. The Radial Electric Field Formation in CERC Plasma

The FORTEC-3D code is applied to a CERC plasma observed in the LHD experiment of # 103619. The heating scenario of # 103619 is shown in Fig. 1. The ECH with two gyrotrons of 77 GHz has been operated and the total injection power of the ECH was 1.34 MW for the discharge. The momentum input by ECH in the parallel direction is not taken into account in simulations here since that is small in this discharge. The time evolution of the electron temperature at the magnetic axis of R = 3.53 m and the line averaged density are also shown in the figure, where R is the major radius. The magnetic field strength at the axis is B_ax = 2.705 T. It is noted that the β value is very low for all the timing of this discharge (β < 0.02 %) due to the low density of the plasma. In FORTEC-3D, the effect of the heating power on the neoclassical transport and the E_r formation is not considered. This is justified by the fact that the nonambipolar flux of energetic particles driven by ECH does not contribute so much to the ambipolar condition, and thus the resultant ambipolar E_r for a similar plasma density as the CERC plasma considered here [1].

The electron temperature of the LHD # 103619 discharge observed by the Thomson scattering are shown in Fig. 2 (a). As shown in the figure, T_e at t = 0.8 s (denoted by *flat*) shows a flat profile over the core region of approximately at ρ < 0.4, a locally flat one at t = 0.9 s (*local flat*), and an eITB one at t = 1.1 s (*eITB*). It can be seen that the local flat temperature profile gradually vanishes as the ECH continues as mentioned in Sec. 1. The ion temperature is not available for the discharge, thus the parabolic profile for T_i is assumed with T_i = 0.4 keV at the magnetic axis for all the timing of the discharge as shown in the Fig. 2 (a). The use of the local neoclassical transport code, DGN/LHD, for $\mathit{\Gamma}_\mathrm{i}$ is justified due to the low T_i of the

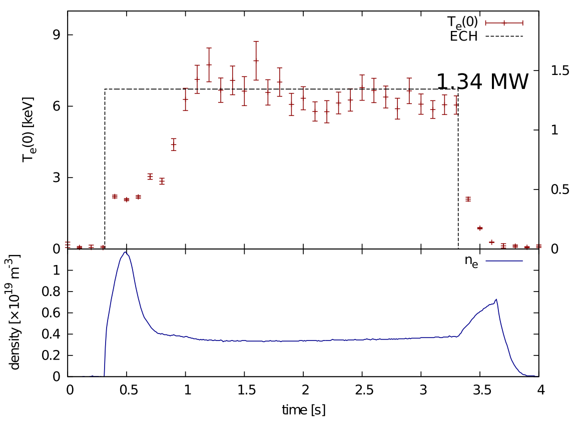

Fig. 1 The time sequence of the ECH of the LHD # 103619 discharge. The total power of 1.34 MW with two 77 GHz gyrotrons was injected for the plasma. The electron temperature at R_ax = 3.53 m and line-averaged density are also shown.

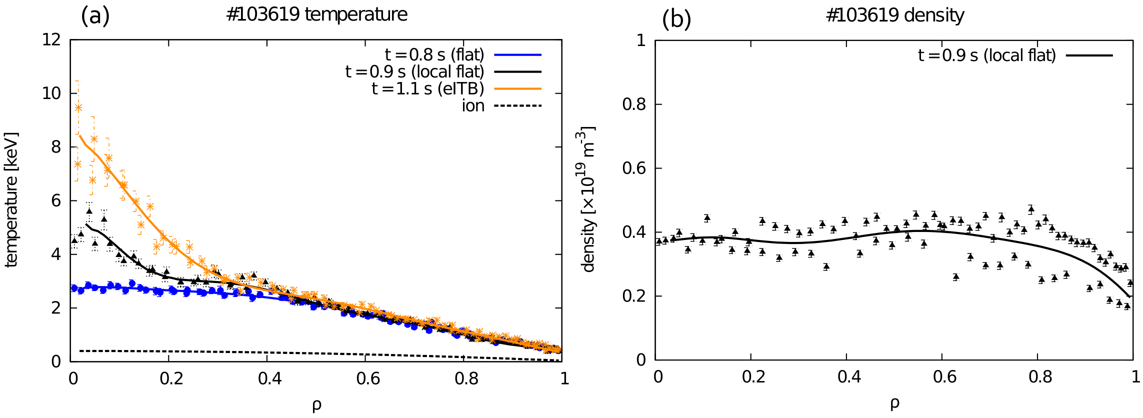

Fig. 2 (a) The temperature profiles of the LHD CERC plasma (# 103619) for several timing. The ion temperature, which is assumed as the same value for all timing due to the lack of the observation, is indicated by a dashed line. (b) The density profile of the discharge. Since the density remains almost constant after $t \simeq 0.8$ s, only the value at $t = 0.9$ s is indicated for simplicity.

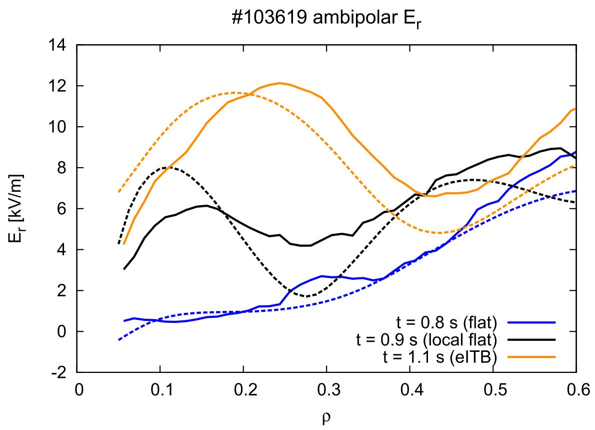

Fig. 3 The ambipolar radial electric field profiles for the LHD CERC plasma obtained by FORTEC-3D. Each E_r profile shows a value at the steady state. The ambipolar E_r obtained by DGN/LHD are also plotted in the figure (dashed lines).

CERC plasma. The plasma density of the discharge is flat and low ($n_e \simeq 0.4 \times 10^{19}$ m^{-3}) as shown in Fig. 2 (b). The plasma density remains almost constant after $t \simeq 0.8$s (see also Fig. 1), thus only the value at $t = 0.9$ s is indicated for simplicity. It is noted that FORTEC-3D calculates the neoclassical transport for fitted profiles of T_e and n_e shown in Figs. 2 (a) and (b) and equilibrium magnetic fields obtained by VMEC code [15].

The FORTEC-3D simulations presented in this paper have used 2×10^7 markers for the lower T_e cases ($t = 0.9$ and 1.0 s) and 4×10^7 for high T_e case ($t = 1.1$ s). Since the larger thermal velocity of the high T_e plasmas can degrade the accuracy of the simulation results, twice as much markers are used in the latter case. For $t = 1.1$ s case, we have confirmed the convergence of simulation results by varying the number of markers $N_m = 1 \times 10^7$, 2×10^7 and 4×10^7. It has been confirmed that the ambipolar E_r is almost unaffected by N_m, and Q_e changes 20 – 30% at most in the core region and is unaffected at $\rho > 0.3$.

The radial electric field obtained by FORTEC-3D is shown in Fig. 3. In this figure, E_r^{F3D} at $t = 0.8$ (denoted by flat), 0.9 (local flat), and 1.1 s (eITB) are shown, respectively. Dashed lines in the figure represent results obtained by DGN/LHD, that is, E_r^{DGN}. As indicated in the figure, the ambipolar electron-root E_r with the steep shear is spontaneously formed along with the eITB formation from $t = 0.8$ to 1.1 s at the core region. In the low T_e plasma at $t = 0.8$ s, the ambipolar E_r of FORTEC-3D and DGN/LHD almost agree with each other. This is because the FOW effect in the low T_e plasma is small so that the electron particle fluxes of both codes are almost the same. On the other hand, the difference between FORTEC-3D and DGN/LHD becomes larger at $t = 1.1$ s when T_e increases especially at around $\rho = 0.14$ where the steep T_e gradient forms, and it results in approximately 20% at the most there.

As described in Sec. 2, the radial electric field is determined by the electron and ion particle fluxes to satisfy the ambipolar condition of $\Gamma_e(E_r, U_{e,\parallel}) = \Gamma_i(E_r, U_{i,\parallel})$. Note here that Γ_e from FORTEC-3D depends implicitly on the electron parallel flow, too. The electron parallel flow, defined as $n_e U_{e,\parallel} = \int v_\parallel \delta f d^3v$ in FORTEC-3D, can be seen as one that evolves according to the $m_e v_\parallel$-moment of the drift kinetic equation (1):

$$m_e n_e \frac{\partial U_{e,\parallel}}{\partial t} = -\langle \boldsymbol{B} \cdot \nabla \cdot \boldsymbol{\Pi}_e \rangle + \langle \boldsymbol{B} \cdot \boldsymbol{F}_e \rangle, \qquad (6)$$

where $\boldsymbol{\Pi}_e$ is the electron viscosity tensor, and $\boldsymbol{F}_e$ is the friction force between electron and ion, respectively. Γ_i in the ambipolar condition is given as a function of the radial position ρ and E_r at each time step in FORTEC-3D from a Γ_i-database made by DGN/LHD code, which determines the steady-state Γ_i without including the ion-electron collision operator due to the small mass ratio $m_e \ll m_i$ (for more detailed description of DGN/LHD, see Ref. [13] and references therein). On the other hand, in the parallel momentum balance for ions, which has a similar form as Eq. (6), the ion-electron friction can be neglected again due to the small mass ratio. Complete momentum balance between ions and electrons is required only to explain the intrinsic ambipolarity in axisymmetric tokamaks. In LHD cases, ion-electron friction term has little effect in determining both ion parallel flow and the ambipolar condition because of finite neoclassical toroidal viscosity $\langle \boldsymbol{B}_\mathrm{t} \cdot \nabla \cdot \boldsymbol{\Pi}_\mathrm{i} \rangle$ in helical plasmas [16]. Moreover, since we analyze here ECH-heated plasmas, there is no explicit momentum source for ion and the assumption $v_\mathrm{th,e} \gg U_\mathrm{i} \simeq 0$ in our model is valid. Therefore, although the Γ_i-database from DGN/LHD code neglects the effect of ion-electron friction, and as a result, our simulation model of FORTEC-3D does not treat the momentum transfer from electron to ion, the use of the Γ_i-database is justified to determine the ambipolar E_r in our simulation model for LHD under the $m_\mathrm{e}/m_\mathrm{i} \to 0$ limit approximation. The electron parallel flow and the E_r such obtained in FORTEC-3D simultaneously satisfy both the ambipolar condition and the parallel momentum balance Eq. (6).

The E_r and the electron mean flow also satisfy the radial force balance relation. The radial force balance relation is obtained from the momentum balance equation and is expressed as follows:

$$E_\psi + \frac{p_\mathrm{e}'}{en_\mathrm{e}} + U^\theta = \frac{\iota}{2\pi} U^\zeta, \tag{7}$$

where the radial electric field is expressed in ψ-coordinate instead of r, p_e' is the pressure gradient, and $U^\theta = \boldsymbol{U} \cdot \nabla\theta$ and $U^\zeta = \boldsymbol{U} \cdot \nabla\zeta$ are contravariant components in theta- and zeta-directions of the electron mean flow, $n\boldsymbol{U} = \int \boldsymbol{v}\delta f \mathrm{d}^3 v$. In the present cases, it is found that $U/v_\mathrm{th,e} \sim O(10^{-4})$ and $U^\zeta/U^\theta < O(10^{-1})$. This makes the U^ζ term in the right hand side of Eq. (7) negligible, leading to the $E_\psi + p_\mathrm{e}'/en_\mathrm{e} + U^\theta \simeq 0$. To see this more in detail, the radial force balance for $t = 1.1$ s case is shown in Fig. 4. As clearly seen in the figure, the sum of the left hand side (black line) is almost zero over the wide region of the plasma, and the U^ζ term contributes little to the force balance (see dashed pink and orange lines in the figure).

The energy flux, Q_e, and the heat diffusivity, $\chi_\mathrm{e}^\mathrm{NC}$ of those plasmas obtained by FORTEC-3D are shown in Figs. 5 (a) and (b). It is noted that the energy flux represents the total heat flux, that is, the sum of the convective and conductive heat fluxes. The energy fluxes calculated by DGN/LHD are also shown by dashed lines in Fig. 5 (a). The difference of the energy flux between FORTEC-3D and DGN/LHD at $t = 0.9$ and 1.1 s are approximately 20 – 30% at $\rho \simeq 0.14$, which is slightly larger than that of E_r. This is explained as follows. Particles used in FORTEC-3D have various energies, while DGN/LHD uses the mono-energetic particle to evaluate the neoclassical transport. Since the energy flux is evaluated by v^2 moment of the particle distribution function δf, the existence of such energy-distributed particles in FORTEC-3D

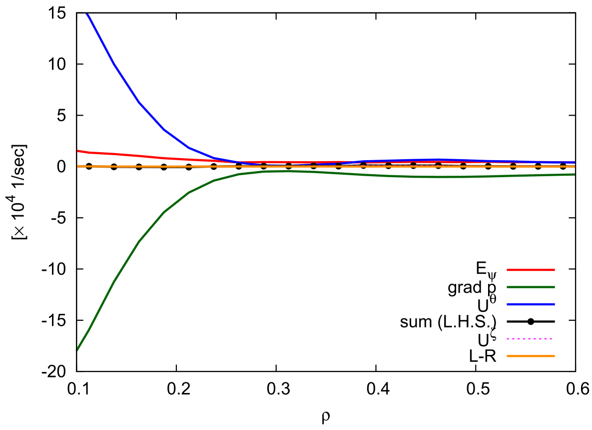

Fig. 4 Force balance relation in LHD plasma of #103619 at $t =$ 1.1 s. In the figure, red line represents the E_ψ term in left hand side of Eq. (7), green the pressure gradient, blue U^θ and black with point the sum of them. Dashed pink line represents the U^ζ term in the right hand side of the same equation, and orange is the difference between black and orange lines. It is noted that the terms shown here are averaged over the magnetic surface.

more affects the energy flux rather than the particle flux and the ambipolar E_r, where the former is the constraint of the ambipolar condition of $\Gamma_\mathrm{e} = \Gamma_\mathrm{i}$. It is noted that the ion particle flux, Γ_i, is evaluated by DGN/LHD. The difference in the energy flux arises from this fact in addition to the difference in the ambipolar E_r seen in Fig. 3. The neoclassical heat diffusivities are shown by solid lines in Fig. 5 (b). It is noted that $\chi_\mathrm{e}^\mathrm{NC}$ shown in the figure represents effective values with respect to this energy flux, and are defined as $\chi_\mathrm{e}^\mathrm{NC} \equiv Q_\mathrm{e}/(-n_\mathrm{e}\nabla T_\mathrm{e})$. Although the energy flux increases due to the increase in T_e, the neoclassical heat diffusivity at the core rather remains low level even when T_e becomes high at $t = 0.9$ and 1.1 s. This is due to the formation of the large electron-root E_r during the eITB formation shown in Fig. 3. With the large electron-root E_r in the CERC plasma, the neoclassical heat diffusivity *does not* show the so-called $1/\nu$ scaling which is expected to be large in high temperature plasmas if $E_\mathrm{r} = 0$. In other words, the spontaneously growing electron-root E_r compensates the $1/\nu$ increase in $\chi_\mathrm{e}^\mathrm{NC}$ when the eITB formation occurs in the CERC plasma. The neoclassical heat diffusivities are compared to experimental values, which are estimated from the power deposition profile of the ECH, in Fig. 5 (b). The experimental heat diffusivities $\chi_\mathrm{e}^\mathrm{EXP}$ at the core are drastically reduced by the order of magnitude of 10^1 or more from $t = 0.8$ s to 1.1 s. Since the neoclassical part of the transport, $\chi_\mathrm{e}^\mathrm{NC}$ remains unchanged during the discharge, the reduction of the experimental heat diffusivity can be mainly attributed to the reduction of the anomalous, or the turbulent transport.

To explore the characteristics of the neoclassical transport further, dependence on the plasma collisionality is

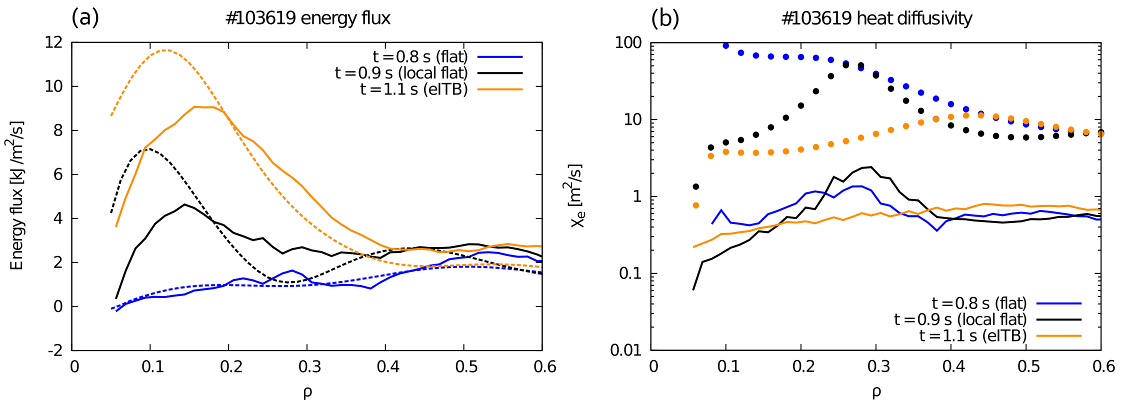

Fig. 5 (a) Radial profiles of the energy flux evaluated by FORTEC-3D (solid lines) and DGN/LHD (dashed lines) at t = 0.8, 0.9 and 1.1 s of the LHD # 103619 discharge. (b) Radial profiles of the neoclassical heat diffusivities, χ_e^{NC} (solid lines) and experimental ones, χ_e^{EXP} (circles). The former ones are obtained by FORTEC-3D and the latter are estimated from the power deposition of the ECH.

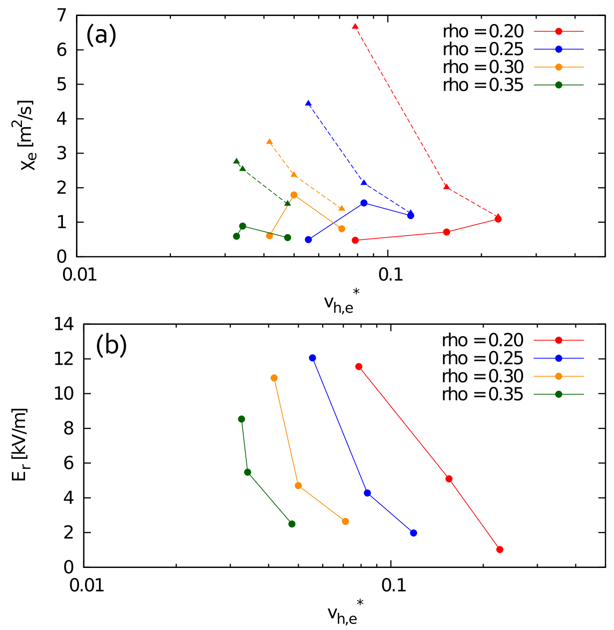

Fig. 6 (a) Neoclassical heat diffusivities evaluated by FORTEC-3D (solid lines with symbols) vs. the normalized collisionality, $\nu^*_{h,e}$ at several radial positions. In (a), dashed lines with symbols corresponds to values with artificially setting E_r = 0. (b) The radial electric field evaluated by FORTEC-3D (solid lines with symbols) vs. the normalized collisionalities at the same positions as those in (a).

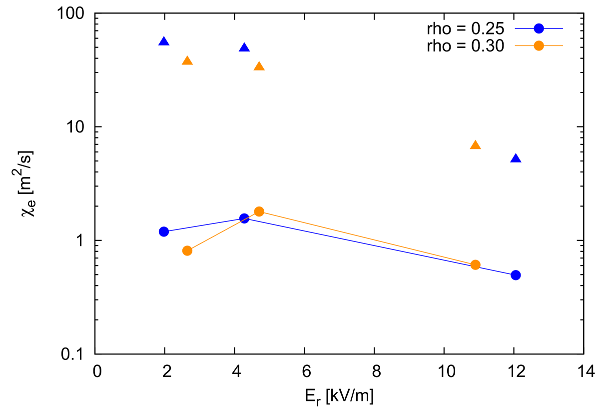

Fig. 7 The Heat diffusivities vs. the radial electric field. Solid lines represent the neoclassical ones obtained by FORTEC-3D, and triangles represent experimental estimations which are the same as those in Fig. 5 (b).

investigated. The heat diffusivities and the ambipolar E_r at several radial positions of ρ = 0.20, 0.25, 0.30 and 0.35 are plotted with the collisionality in Figs. 6 (a) and (b). The normalized collisionality is defined as $\nu^*_{h,e} = \nu / \left[\epsilon_h^{3/2}(v_{th,e}/qR)\right]$, where ν denotes the collision frequency, and ϵ_h and q are the helicity of the LHD magnetic configuration and the safety factor, respectively. For comparisons with the $1/\nu$-type dependence of the heat diffusivity, χ_e^{NC} evaluated from DGN/LHD by setting E_r = 0 are also plotted by dashed lines in the Fig. 6 (a). It is clearly shown in the figure that χ_e^{NC} clearly decreases due to the larger value of E_r as the collisionality (T_e) decreases (increases), see solid lines in Figs. 6 (a) and (b). It can be concluded that the $1/\nu$ dependence of the heat diffusivity is clearly avoided at all the radial positions with the formation of the electron-root E_r when the collisionality becomes low. This shows that the neoclassical heat diffisivity results in either $\sqrt{\nu}$- or ν-regime with the ambipolar E_r instead of $1/\nu$-regime. Figure 7 shows the dependence of both χ_e^{NC} and χ_e^{EXP} on the ambipolar E_r realized at ρ = 0.25 and 0.30. One can see the clear reduction of the experimental heat diffusivity in the figure, while the neoclassical heat diffusivities at both positions almost remain constants during the discharge in spite of the increase in T_e there.

4. Summary and Discussion

To investigate the radial electric field and its effect on the electron neoclassical thermal transport in a LHD CERC plasma, we have performed the neoclassical transport analyses using FORTEC-3D, which evaluates the neoclassical transport and the ambipolar E_r including the electron FOW effect. The CERC plasma is characterized by the high electron temperature ($T_e > 8$ keV at the core) with the steep gradient of the eITB and the large positive E_r, or the electron root with its steep shear. As pointed out in Ref. [7], the high T_e in a CERC plasma requires the electron FOW effect included in neoclassical transport analyses, and FORTEC-3D is appropriate tool for this purpose. It should be emphasized that this is the first attempt of the neoclassical transport analysis with the electron FOW for such a high T_e CERC plasma in LHD.

The radial electric field shows the spontaneous formation resulting in the large electron-root value with the eITB formation in the CERC plasma. The resultant χ_e^{NC} remains unchanged and kept lower values over the entire region inside the eITB foot point although the neoclassical thermal transport itself increases along with the increase in T_e. This indicates that the spontaneous formation of the large electron-root E_r compensates the $1/\nu$ degrading of the neoclassical transport. At the same time, the experimental heat diffusivity shows a clear reduction by the order of 10 or so during the eITB formation although it still remains much larger than the neoclassical transport level.

The ETG turbulence is attributed to the remaining transport since the steep T_e gradient exists in the CERC plasma. The effect of the $\boldsymbol{E} \times \boldsymbol{B}$ velocity shear on the growth of the turbulence plays a significant role for the transport reduction, see a review paper by Burrell [17] and references therein. Also it has been shown experimentally that the suppression of the turbulence-driven transport by the $\boldsymbol{E} \times \boldsymbol{B}$ velocity shear results in the transport barrier in helical devices [18]. As described above, the considerable reduction of the transport accomplished in the CERC plasma is realized with the spontaneous formation of the electron-root E_r with the large shear. Therefore, it can be expected that either the neoclassical ambipolar E_r and/or its shear results in the improved confinement of the CERC plasma. It is required to investigate either of these mechanisms more contribute to the reduction of the turbulent transport in the CERC plasma: the large electron-root E_r itself or the steep E_r shear at the eITB region. The linear growth rate of the ETG turbulence obtained by a gyrokinetic transport code, GKV-X [19], will be compared to the E_r shearing rate to discuss the turbulent transport in the CERC plasma in a forthcoming paper.

Acknowledgments

The authors would like to acknowledge Prof. Hideo Sugama (NIFS) for fruitful discussions on the transport physics in helical plasmas. This work is supported in part by JSPS Grant-in-Aid for Young Scientists (B), No. 23760810 and in part by the NIFS Collaborative Research Programs, NIFS12KNST038.

[1] K. Ida *et al*., Phys. Rev. Lett. **91**, 085003 (2003).
[2] M. Yokoyama *et al*., Fusion Sci. Technol. **50**, 327 (2006).
[3] T. Shimozuma *et al*., Nucl. Fusion **45**, 1396 (2005).
[4] H. Takahashi *et al*., IAEA Fusion Energy Conference 2010, pp. EXC/P8, Daejon, Korea (2010).
[5] T. Shimozuma *et al*., J. Phys.: Conf. Series **123**, 012022 (2008).
[6] M. Yokoyama *et al*., Nucl. Fusion **47**, 1213 (2007).
[7] S. Matsuoka *et al*., Phys. Plasmas **18**, 032511 (2011).
[8] A.H. Boozer, Phys. Fluids **24**, 1999 (1981).
[9] S. Brunner *et al*., Phys. Plasmas **6**, 4504 (1999).
[10] W.X. Wang *et al*., J. Plasma Fusion Res. SERIES **2**, 250 (1999).
[11] S. Satake *et al*., Plasma Fusion Res. **3**, S1062 (2008).
[12] W.I. van Rij and S.P. Hirshman, Phys. Fluids B **1**, 563 (1989).
[13] A. Wakasa *et al*., Contrib. Plasma Phys. **50**, 582 (2010).
[14] S. Matsuoka *et al*., Plasma Fusion Res. **6**, 1203016 (2011).
[15] S.P. Hirshman and O. Betancourt, J. Comput. Phys. **96**, 99 (1991).
[16] H. Sugama *et al*., Plasma Phys. Control. Fusion **53**, 024004 (2011).
[17] K.H. Burrell, Phys. Plasmas **4**, 1499 (1997).
[18] A. Fujisawa *et al*., Plasma Phys. Control. Fusion **48**, S205 (2006).
[19] M. Nunami *et al*., Plasma Fusion Res. **5**, 016 (2010).